robotics

MDPI

Article

Eight-Bar Elbow Joint Exoskeleton Mechanism

Giorgio Figliolini [1,*], Chiara Lanni [1], Luciano Tomassi [1] and Jesús Ortiz [2]

[1] Department of Civil and Mechanical Engineering (DiCEM), University of Cassino and Southern Lazio, 03043 Cassino, Italy; chiara.lanni@unicas.it (C.L.); luciano.tomassi@unicas.it (L.T.)
[2] Department of Advanced Robotics (ADVR), Istituto Italiano di Tecnologia (IIT), 16163 Genoa, Italy; jesus.ortiz@iit.it
* Correspondence: giorgio.figliolini@unicas.it

Abstract: This paper deals with the design and kinematic analysis of a novel mechanism for the elbow joint of an upper-limb exoskeleton, with the aim of helping operators, in terms of effort and physical resistance, in carrying out heavy operations. In particular, the proposed eight-bar elbow joint exoskeleton mechanism consists of a motorized Watt I six-bar linkage and a suitable RP dyad, which connects mechanically the external parts of the human arm with the corresponding forearm by hook and loop velcro, thus helping their closing relative motion for lifting objects during repetitive and heavy operations. This relative motion is not a pure rotation, and thus the upper part of the exoskeleton is fastened to the arm, while the lower part is not rigidly connected to the forearm but through a prismatic pair that allows both rotation and sliding along the forearm axis. Instead, the human arm is sketched by means of a crossed four-bar linkage, which coupler link is considered as attached to the glyph of the prismatic pair, which is fastened to the forearm. Therefore, the kinematic analysis of the whole ten-bar mechanism, which is obtained by joining the Watt I six-bar linkage and the RP dyad to the crossed four-bar linkage, is formulated to investigate the main kinematic performance and for design purposes. The proposed algorithm has given several numerical and graphical results. Finally, a double-parallelogram linkage, as in the particular case of the Watt I six-bar linkage, was considered in combination with the RP dyad and the crossed four-bar linkage by giving a first mechanical design and a 3D-printed prototype.

Keywords: upper-limb exoskeleton; elbow joint; multi-loop mechanisms; kinematic analysis; mechanical design

check for updates

Citation: Figliolini, G.; Lanni, C.; Tomassi, L.; Ortiz, J. Eight-Bar Elbow Joint Exoskeleton Mechanism. *Robotics* **2024**, *13*, 125. https://doi.org/10.3390/robotics13090125

Academic Editor: Kean C. Aw

Received: 4 July 2024
Revised: 14 August 2024
Accepted: 21 August 2024
Published: 23 August 2024

Copyright: © 2024 by the authors. Licensee MDPI, Basel, Switzerland. This article is an open access article distributed under the terms and conditions of the Creative Commons Attribution (CC BY) license (https://creativecommons.org/licenses/by/4.0/).

1. Introduction

Exoskeleton design, in particular for devices like upper limb exoskeletons, is aimed to carefully replicate the human joint movements. Achieving this accuracy involves understanding the kinematics of the human body and translating it into appropriate mathematical models. This, together with an adequate fit, size, and weight, determines the goodness of the designed device itself. In order to be able to design these devices, it is therefore necessary to first understand what the real movements are and make an appropriate schematization. In particular, the human arm is composed of three joints: the shoulder, the elbow, and the wrist. From a kinematic point of view, the human arm can be schematized with an open kinematic chain with 7 degrees of freedom (DOF), as reported in [1,2]. Specifically, there are 3 DOF in the shoulder (ball and socket joint), 1 DOF in the elbow (revolute joint), and 3 DOF in the wrist (spherical joint). Among the upper limb exoskeletons there are many examples of 7 DOF kinematic chains, which try to reproduce the real kinematic scheme of the human arm [3,4], but there are also examples of kinematic chains with a lower number of degrees of freedom, such as those at 3 DOF [5,6] or 6 DOF [7,8]. Over the years, exoskeletons have undergone considerable variations not only in terms of choice of kinematic chain but also in terms of fields of application. In fact, historically, they were born in the military field with the aim of increasing the performance of soldiers in terms of resistance and strength, but

are widely used both in the rehabilitation and in the industrial fields. In particular, in the rehabilitation sector, upper limb exoskeletons have undergone considerable development in the last decade [9–14]. Exoskeletons for the upper limb also differ in relation to the actuation system. Considering that they can also be totally passive or underactuated, most of them have electric actuation [15], even if there are also examples of exoskeletons that have a pneumatic actuation [16]. In the design of upper limb exoskeletons, different types of mechanisms are used. They typically present serial kinematic chains, but there are also examples of exoskeletons that have parallel architectures [17], rather than the presence of gears [18] or tendon-driven systems [19,20].

In recent years, it is also possible to find an effort in the design of systems that are as anthropomorphic, as possible, as proposed by Bai in [21] regarding the shoulder joint which approximates a spherical motion. The synthesis of a spherical rigid body guidance for five-poses can be found in [22]. Furthermore, soft robotics has been gaining traction in the field of exoskeletons. Soft robotic exosuits provide a comfortable and portable alternative to rigid exoskeletons for upper limb support, enhancing user comfort and freedom of movement, as reported in [23].

Also, with regard to the elbow, there are several solutions that try to consider the fact that it cannot strictly be represented with a simple revolute joint [24–29]. It is clear that in order to design a mechanism that is able to approximate as faithfully as possible the real movement of the human elbow, it is necessary to perform an accurate analysis of the movement. For this purpose, centrodes, which represent the exact law of motion that the designer wants to approximate, are useful.

In the literature, Beadle and O'Brien conducted the first experiments on the experimental detection of the human elbow centrodes [30], taking inspiration from Freudenstein, who years earlier had pioneered the usefulness of centrodes in the analysis of human knee movement [31]. The use of centrodes as a kinematic analysis tool can be found in different fields of engineering. As proposed by the authors in [32], centrodes can be used as an analysis tool to validate knee joint exoskeleton mechanism accuracy. They can also be used to investigate the kinematic characteristics of classical mechanisms, but their field of application is transversal and also related to other sectors, such as machine tools [33]. This analysis tool, combined with that of the Bresse circles [34,35] can be very useful for the designer when designing new devices.

The subject of this paper is the design and the kinematic analysis of a novel eight-bar elbow joint exoskeleton mechanism that is composed by a motorized Watt I six-bar linkage and a suitable RP dyad, which connects mechanically the external parts of the human arm with the corresponding forearm by hook and loop velcro. Moreover, the human arm is sketched by means of a crossed four-bar linkage, which coupler link is considered as attached to the glyph of the prismatic pair, which is fastened to the forearm.

Therefore, the kinematic analysis of the whole ten-bar mechanism is formulated to investigate the main kinematic performance and for design purposes. The proposed algorithm has given several numerical and graphical results, and finally, a double-parallelogram linkage was considered in combination with the RP dyad and the crossed four-bar linkage by giving a first mechanical design and a 3D-printed prototype.

The main benefits of the proposed eight-bar elbow joint exoskeleton mechanism are:

- A natural coupling with the human arm;
- Wearable by workers of different arm sizes;
- One motor only;
- A comfortable motor installation under the human arm.

2. Ten-Bar Exoskeleton Elbow Joint Mechanism

The whole one DOF upper-limb exoskeleton mechanism that includes the kinematic sketch of the human arm is represented by the ten-bar mechanism of Figure 1, which consists of the proposed eight-bar elbow joint exoskeleton mechanism and the crossed four-bar linkage. In particular, the first is composed by the Watt I six-bar linkage, which

links are numbered by 1 to 6, and the RP dyad of members 6 (coupler), 7 (piston), and 8 (glyph). When the eight-bar elbow joint exoskeleton mechanism is worn, links 1 and 8 are fastened by hook and loop velcro to the arm and forearm, respectively.

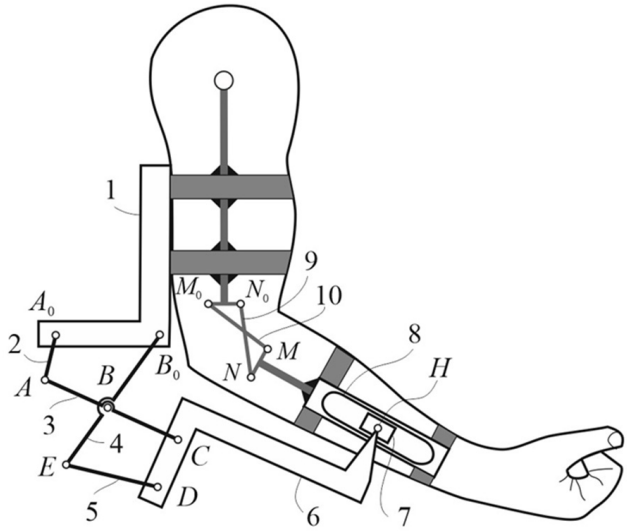

Figure 1. Ten-bar exoskeleton elbow joint mechanism.

The human elbow joint is made up of three bones: the upper arm bone (humerus) and two forearm bones (ulna and radius), which can be sketched by a crossed four-bar linkage of links 1 (arm) and 8 (forearm), along with the crossed links 9 and 10. In fact, the relative motion is not a pure rotation and thus, the upper part of the exoskeleton is fastened to the arm, while the lower part is not rigidly connected to the forearm.

The macroscopic movement of the elbow is actually the result of the interaction between the ends of the bony segments of the arm and forearm in contact. They can be thought of as conjugate surfaces; the relative movement between these two represents the effective motion law of the elbow. If one approaches the movement of the elbow as a plane movement, the projections of these surfaces on it are two curves, which represent the centrodes, whose point of contact is the instantaneous center of rotation. The use of a crossed-four-bar linkage allows to have the position of the instantaneous center of rotation of the coupler link 8 (glyph) close to that of the forearm with respect to the arm.

Applying Grubler's formula, one has

$$N = 3\,(n-1) - 2l = 27 - 13 \cdot 2 = 1 \text{ DOF} \tag{1}$$

where N, n, and l are the numbers of the degrees of freedom of the rigid links and of the lower kinematic pairs, respectively.

In the following, the kinematic analysis of the human elbow joint and its exoskeleton is formulated.

3. Kinematic Analysis

The kinematic analysis of the one DOF ten-bar mechanism of Figure 2 is developed by first considering separately the Watt I six-bar linkage A_0ABB_0-$BCDE$ and the crossed four-bar linkage M_0MNN_0, respectively, and then joining them at H point to analyze the whole ten-bar mechanism. This chapter is organized in the following three sub-sections:

- Watt I six-bar linkage
- Crossed four-bar linkage
- Ten-bar mechanism

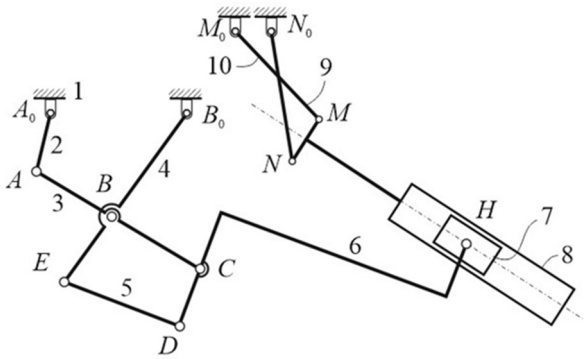

Figure 2. Ten-bar mechanism.

3.1. Watt I Six-Bar Linkage

The main part of the proposed elbow joint exoskeleton mechanism is the Watt I six-bar linkage of Figure 3a, which includes the vector loops of both four-bar linkages A_0ABB_0 and $BCDE$ by giving the following vector equations:

$$\begin{aligned} \mathbf{r}_2 + \mathbf{r}_{31} - \mathbf{r}_1 - \mathbf{r}_{41} &= \mathbf{0} \\ \mathbf{r}_{42} + \mathbf{r}_5 - \mathbf{r}_{32} - \mathbf{r}_6 &= \mathbf{0} \end{aligned} \tag{2}$$

where vectors $\mathbf{r}_i$ are expressed by $\mathbf{r}_i = (r_i \cos\theta_i)\mathbf{i} + (r_i \sin\theta_i)\mathbf{j}$ for i = 1, . . ., 6, where $\mathbf{i}$ and $\mathbf{j}$ are the unit vectors of the X and Y-axes. The same is for the vectors $\mathbf{r}_{31}$, $\mathbf{r}_{32}$, $\mathbf{r}_{41}$ and $\mathbf{r}_{42}$ which second subscript number refers to loops 1 and 2, respectively.

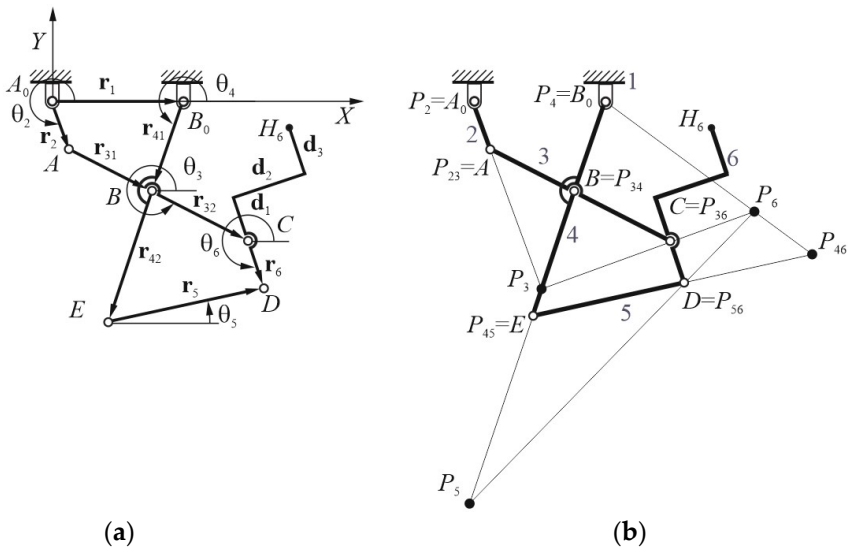

Figure 3. Watt I six-bar linkage: (**a**) vector loops; (**b**) ICs.

The ICs (instantaneous centers of rotation) P_3, P_5 and P_6 of the coupler links 3, 5 and 6, respectively, have been determined by applying the Aronhold-Kennedy theorem, according to the graphical constructions of Figure 3b.

Thus, the first of Equation (2) gives

$$\mathcal{A} sin\theta_3 + \mathcal{B}\cos\theta_3 + \mathcal{C} = 0 \tag{3}$$

which can be solved as follows

$$\theta_3 = 2tan^{-1}\frac{-\mathcal{A} + \sigma\sqrt{\mathcal{A}^2 - \mathcal{C}^2 + \mathcal{B}^2}}{\mathcal{C} - \mathcal{B}} \tag{4}$$

where σ is equal to ±1 according to the assembly mode.

The coefficients $\mathcal{A}$, $\mathcal{B}$ and $\mathcal{C}$ are obtained as function of the driving angle θ_2 by

$$\begin{aligned} \mathcal{A} &= 2\, r_2\, r_{31} \sin\theta_2 \\ \mathcal{B} &= 2\, r_{31}(r_2 \cos\theta_2 - r_1) \\ \mathcal{C} &= r_1^2 + r_2^2 + r_{31}^2 - r_{41}^2 - 2\ r_1\, r_2 \cos\theta_2 \end{aligned} \tag{5}$$

Moreover, solving the first of Equation (2) with respect to θ_4, one has

$$\theta_4 = \tan^{-1} \frac{r_{31} \sin\theta_3 + r_2 \sin\theta_2}{r_2 \cos\theta_2 + r_{31} \cos\theta_3 - r_1} \tag{6}$$

From the first of Equation (2), the angular velocities ω_3 and ω_4 can be obtained as follows

$$\begin{aligned} \omega_4 &= \tfrac{r_2 \sin(\theta_2-\theta_3)}{r_{41} \sin(\theta_4-\theta_3)} \omega_2 \\ \omega_3 &= \tfrac{r_2 \sin(\theta_2-\theta_4)}{r_{31} \sin(\theta_4-\theta_3)} \omega_2 \end{aligned} \tag{7}$$

where the angles θ_3 and θ_4 are given by Equations (4) and (6), respectively.

Similarly, from the second of Equation (2), one has

$$\theta_6 = 2tan^{-1} \frac{-\mathcal{D} + \sigma\sqrt{\mathcal{D}^2 - \mathcal{F}^2 + \mathcal{E}^2}}{\mathcal{F} - \mathcal{E}} \tag{8}$$

which the coefficients $\mathcal{D}$, $\mathcal{E}$ and $\mathcal{F}$ are given by

$$\begin{aligned} \mathcal{D} &= 2\, r_{32}\, r_6 \sin\theta_3 - 2\, r_{42}\, r_6 \sin\theta_4 \\ \mathcal{E} &= 2\, r_{32}\, r_6 \cos\theta_3 - 2\, r_{42}\, r_6 \cos\theta_4 \\ \mathcal{F} &= r_{42}^2 + r_{32}^2 + r_6^2 - r_5^2 - 2\, r_{42}\, r_{32} \cos\theta_3 \cos\theta_4 - 2\, r_{42}\, r_{32} \sin\theta_3 \sin\theta_4 \end{aligned} \tag{9}$$

Thus, solving with respect to θ_5, one has

$$\theta_5 = \tan^{-1} \frac{r_{32} \sin\theta_3 + r_6 \sin\theta_6 - r_{42} \sin\theta_4}{r_{32} \cos\theta_3 + r_6 \cos\theta_6 - r_{42} \cos\theta_4} \tag{10}$$

From the second of Equation (2), the angular velocities ω_5 and ω_6 are obtained as follows

$$\omega_5 = \frac{\omega_3\, r_{32} \sin(\theta_6 - \theta_3) - \omega_4\, r_{42} \sin(\theta_6 - \theta_4)}{r_5 \sin(\theta_6 - \theta_5)} \tag{11}$$

$$\omega_6 = \frac{\omega_3\, r_{32} \sin(\theta_5 - \theta_3) - \omega_4\, r_{42} \sin(\theta_5 - \theta_4)}{r_6 \sin(\theta_6 - \theta_5)} \tag{12}$$

The velocity vectors $\mathbf{v}_A$, $\mathbf{v}_B$, $\mathbf{v}_C$, $\mathbf{v}_D$ and $\mathbf{v}_E$ of points A, B, C, D and E, respectively, are obtained by assuming the following in vector forms:

$$\begin{aligned} \mathbf{v}_A &= \omega_2 \left[\ -r_2\ \sin\theta_2, \quad r_2\ \cos\theta_2\ \right]^T \\ \mathbf{v}_B &= \omega_4 \left[\ -r_4\ \sin\theta_4, \quad r_4\ \cos\theta_4\ \right]^T \\ \mathbf{v}_C &= \left[\ v_{BX} - r_{32}\, \omega_3 \sin\theta_3, \quad v_{BY} + r_{32}\, \omega_3 \cos\theta_3\ \right]^T \\ \mathbf{v}_D &= \left[\ v_{CX} - r_6\, \omega_6 \sin\theta_6, \quad v_{CY} + r_6\, \omega_6 \cos\theta_6\ \right]^T \\ \mathbf{v}_E &= \left[\ v_{BX} - r_{42}\, \omega_4 \sin\theta_4, \quad v_{BY} + r_{42}\, \omega_4 \cos\theta_4\ \right]^T \end{aligned} \tag{13}$$

where T indicates the transpose matrix.

Finally, the velocity vector $\mathbf{v}_{H6}$ of the point H, as belonging to the coupler link 6, is given by

$$\mathbf{v}_{H6} = \left[v_{CX} + \omega_6(d_1 + d_3)\ \sin\theta_6 - \omega_6\, d_2 \cos\theta_6, \quad v_{CY} - \omega_6(d_1 + d_3)\ \cos\theta_6 - \omega_6\, d_2 \sin\theta_6\right]^T \tag{14}$$

3.2. Crossed Four-Bar Linkage

The crossed four-bar linkage of Figure 4a, which includes the corresponding vector loop of the linkage M_0MNN_0, sketches the human elbow joint, while Figure 4b shows the graphical construction for determining the ICs of each link.

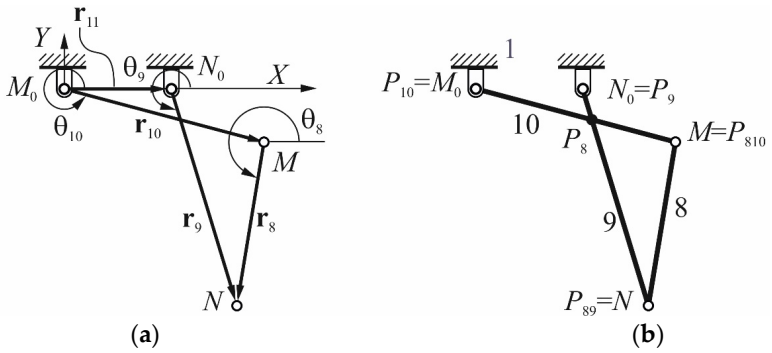

Figure 4. Crossed four-bar linkage: (**a**) vector loop; (**b**) ICs.

Therefore, the following vector-loop equation is obtained

$$\mathbf{r}_{10} + \mathbf{r}_8 - \mathbf{r}_9 - \mathbf{r}_{11} = 0 \tag{15}$$

where $\mathbf{r}_i = (r_i \cos\theta_i)\mathbf{i} + (r_i \sin\theta_i)\mathbf{j}$ for i = 8, . . ., 11.

Thus, one has

$$\mathcal{G}\sin\theta_8 + \mathcal{H}\cos\theta_8 + \mathcal{I} = 0 \tag{16}$$

which can be solved by giving

$$\theta_8 = 2\tan^{-1}\frac{-\mathcal{G} + \sigma\sqrt{\mathcal{G}^2 - \mathcal{I}^2 + \mathcal{H}^2}}{\mathcal{I} - \mathcal{H}} \tag{17}$$

where σ is equal to ±1 according to the assembly mode.

The coefficients $\mathcal{G}$, $\mathcal{H}$ and $\mathcal{I}$ are given as function of the driving crank angle θ_{10} by

$$\begin{aligned} \mathcal{G} &= 2\, r_{10}\, r_8 \sin\theta_{10} \\ \mathcal{H} &= 2\, r_8 (r_{10}\cos\theta_{10} - r_{11}) \\ \mathcal{I} &= r_{11}^2 + r_{10}^2 + r_8^2 - r_9^2 - 2\; r_{10}\, r_{11}\cos\theta_{10} \end{aligned} \tag{18}$$

Moreover, Equation (15) can be solved with respect to θ_9 by giving

$$\theta_9 = \tan^{-1}\frac{r_{11}\sin\theta_{11} + r_8\sin\theta_8 - r_{10}\sin\theta_{10}}{r_{11}\cos\theta_{11} + r_8\cos\theta_8 - r_{10}\cos\theta_{10}} \tag{19}$$

From the Equation (15), the angular velocities ω_8 and ω_9 are obtained as follows

$$\begin{aligned} \omega_8 &= \frac{r_{10}\sin(\theta_{10}-\theta_9)}{r_8\sin(\theta_9-\theta_8)}\omega_{10} \\ \omega_9 &= \frac{r_{10}\sin(\theta_{10}-\theta_8)}{r_9\sin(\theta_9-\theta_8)}\omega_{10} \end{aligned} \tag{20}$$

The velocity vectors of points M and N are given by

$$\begin{aligned} \mathbf{v}_M &= \omega_{10}\left[-r_{10}\,\sin\theta_{10},\quad r_{10}\,\cos\theta_{10}\right]^T \\ \mathbf{v}_N &= \omega_9\left[-r_9\,\sin\theta_9,\quad r_9\,\cos\theta_9\right]^T \end{aligned} \tag{21}$$

3.3. Ten-Bar Mechanism

The formulation that has been developed in the previous two sub-sections is now combined in order to obtain a general algorithm for the kinematic analysis of the whole ten-

bar mechanism. Additional kinematic considerations are applied by using the Aronhold-Kennedy theorem, as shown in Figure 5. In particular, the ICs P_6, P_8, and P_{68} are of interest in order to express the velocity vectors $\mathbf{v}_{H6}$ and $\mathbf{v}_{H8}$ of point H as belonging to the coupler links 6 and 8, respectively, along with their relative velocity vector $\mathbf{v}_{H68}$.

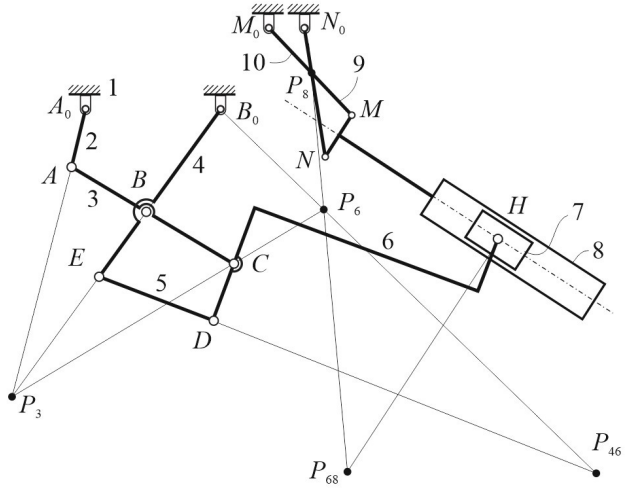

Figure 5. Ten-bar mechanism: ICs.

Thus, one has

$$\mathbf{v}_{H6} = v_{H8} + v_{H68} \tag{22}$$

where each velocity vector is given by

$$\begin{aligned} \mathbf{v}_{H8} &= \omega_{\ 8} \times P_8\, H \\ \mathbf{v}_{H6} &= \omega_{\ 6} \times P_6\, H \\ \mathbf{v}_{H68} &= \omega_{\ 68} \times P_{68}\, H \end{aligned} \tag{23}$$

Therefore, in scalar form, one has

$$\omega_6\, P_6 P_{68} = \omega_8\, P_8 P_{68} \tag{24}$$

where P_6P_{68} and P_8P_{68} are the distances of the ICs P_6 and P_8 with respect to P_{68}.

The angular velocity ω_8 of the coupler link 8 of the four-bar linkage is now related to that of the coupler link 6 of the Watt I six-bar linkage by means of the ICs P_6, P_8 and P_{68}.

4. Graphical and Numerical Results

The proposed formulation for the kinematic analysis of the ten-bar mechanism, which includes both the eight-bar elbow joint exoskeleton mechanism and the human elbow joint mechanism, has been implemented in Matlab for validation purposes.

In fact, Figures 6 and 7 show the results for the crank angles θ_2 = 255° and θ_2 = 290° by giving the angular velocities of all moving links and the linear velocities of points A, B, C, D, E, H, M and N. The geometric input data are reported in Table 1, where the link lengths of the Watt I six-bar linkage, have been chosen in such a way to be compatible with the application as elbow joint exoskeleton mechanism and with the aim to validate, in general, the proposed kinematic analysis algorithm.

Table 1. The geometric input data in the case of Figures 6 and 7.

r_1 [mm]	$r_2 = r_6$ [mm]	r_{31} [mm]	r_{32} [mm]	r_{41} [mm]	r_{42} [mm]
70	30	45	50	65	40
r_8 [mm]	**r_9 [mm]**	**r_{10} [mm]**	**r_{11} [mm]**	**$d_1 = d_3$ [mm]**	**d_2 [mm]**
25	65	60	18	30	117.50

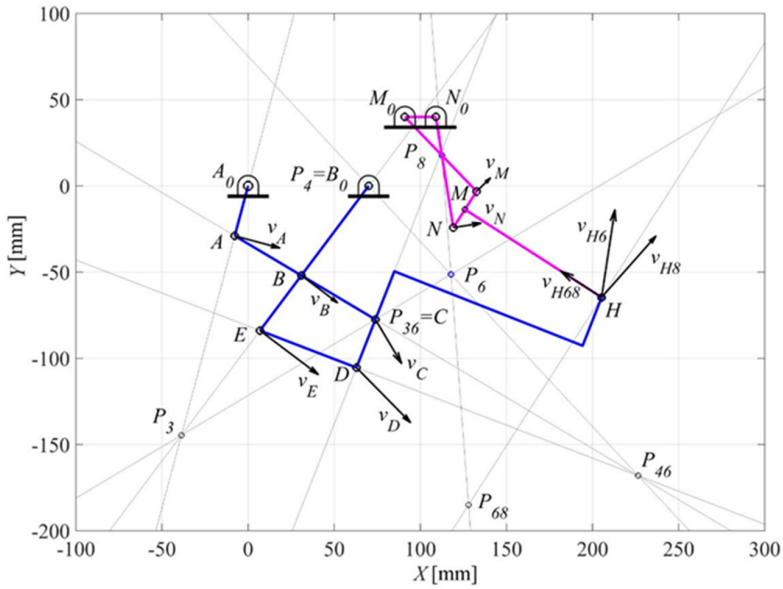

Figure 6. Ten-bar mechanism: result for a crank angle θ_2 = 255° of A_0A (Blue and magenta colors indicate the eight-bar elbow joint exoskeleton mechanism and the crossed four-bar linkage, respectively).

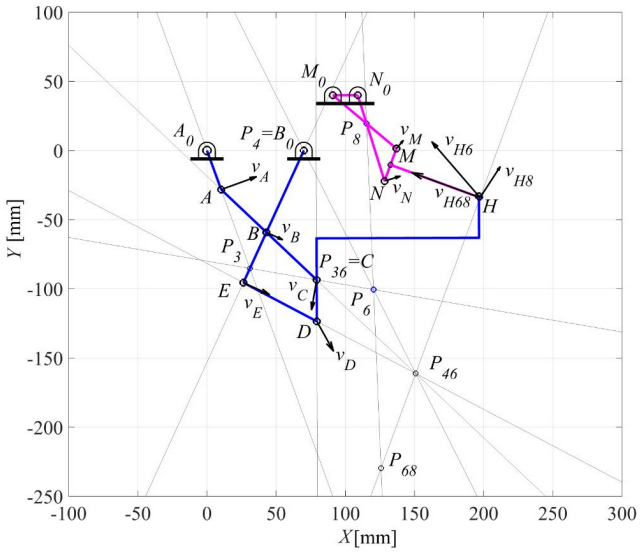

Figure 7. Ten-bar mechanism: result for a crank angle θ_2 = 290° of A_0A.(Blue and magenta colors indicate the eight-bar elbow joint exoskeleton mechanism and the crossed four-bar linkage, respectively).

The results of the proposed algorithm for the input data of Table 1 and the driving angular velocity ω_2 = 1 rad/s, are reported in Tables 2 and 3.

Table 2. Output linear velocities of all significant points for the case of Figures 6 and 7.

θ_2 [deg]	$\mathbf{v}_A$ [mm/s]	$\mathbf{v}_B$ [mm/s]	$\mathbf{v}_C$ [mm/s]	$\mathbf{v}_D$ [mm/s]	$\mathbf{v}_E$ [mm/s]
255	$[28.978, -7.765]^T$	$[23.220, -17.463]^T$	$[16.82, -28.239]^T$	$[34.78, -35.324]^T$	$[37.509, -28.21]^T$
290	$[28.191, 10.261]^T$	$[12.906, -5.905]^T$	$[-4.077, -23.86]^T$	$[13.328, -23.80]^T$	$[20.848, -9.538]^T$
	$\mathbf{v}_{H6}$ [mm/s]	$\mathbf{v}_{H8}$ [mm/s]	$\mathbf{v}_{H68}$ [mm/s]	$\mathbf{v}_M$ [mm/s]	$\mathbf{v}_N$ [mm/s]
255	$[8.648, 56.278]^T$	$[34.933, 39.356]^T$	$[-26.38, 16.937]^T$	$[8.853, 8.549]^T$	$[17.782, 2.818]^T$
290	$[-39.128, 44.18]^T$	$[16.092, 24.658]^T$	$[-54.675, 20.00]^T$	$[5.443, 6.483]^T$	$[12.502, 3.904]^T$

Table 3. Output angular velocities of all moving links for the case of Figures 6 and 7.

θ_2 [deg]	ω_3 [rad/s]	ω_4 [rad/s]	ω_5 [rad/s]	ω_6 [rad/s]	ω_8 [rad/s]	ω_9 [rad/s]	ω_{10} [rad/s]	ω_{11} [rad/s]
255	−0.251	0.447	−0.127	0.644	0.424	0.277	0.205	0.219
290	−0.4944	0.2183	−0.2688	0.5802	0.3007	0.2015	0.1411	0.2795

5. Application and Prototype

The proposed general formulation for the kinematic analysis of the ten-bar mechanism of Figure 2 can be used to analyze and design a suitable eight-bar elbow joint exoskeleton mechanism of different shapes and sizes. In particular, the case of when the Watt I six-bar linkage becomes a double-parallelogram linkage and the crossed four-bar linkage becomes an anti-parallelogram linkage is now considered, and the whole mechanism takes the shape of Figure 8a, according to the application that is sketched in Figure 8b, which also shows both lengths a and b of the lower and upper human arms.

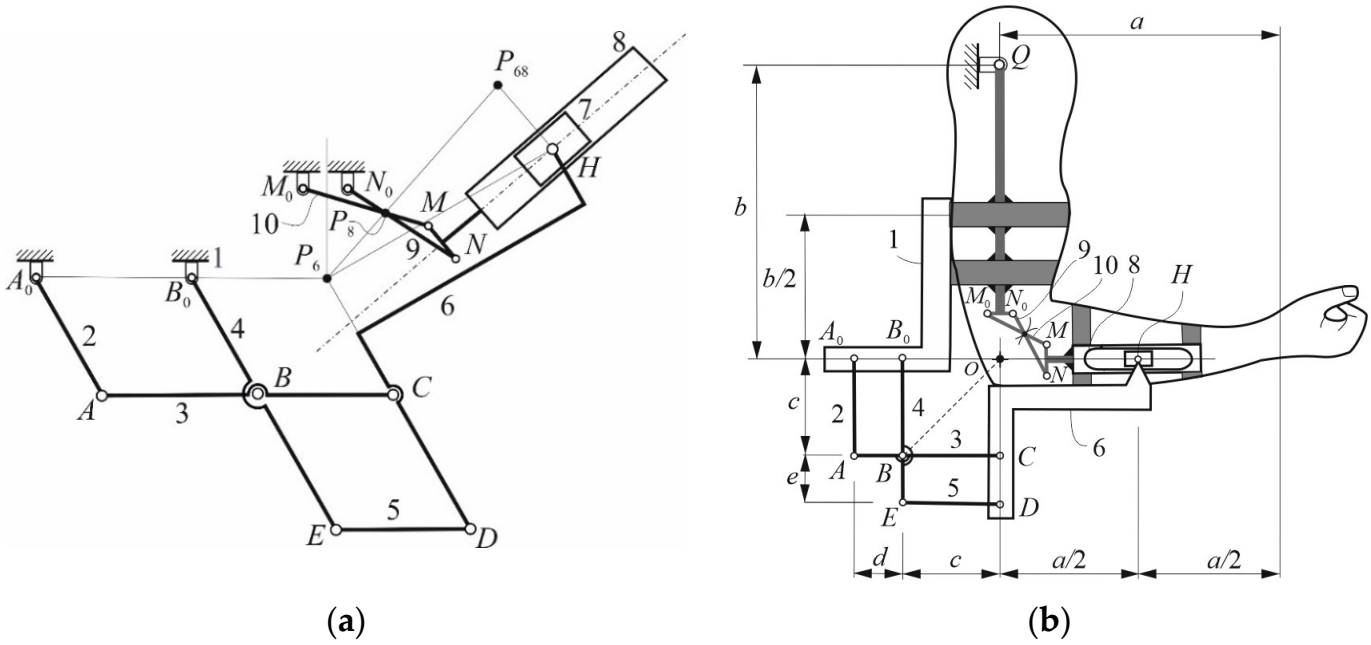

Figure 8. Ten-bar elbow joint exoskeleton mechanism: (**a**) kinematic sketch; (**b**) application.

According to what was reported in [36], the mean values of a = 241 mm and b = 338 mm have been assumed, where each of them has been calculated as the arithmetic mean between the maximum and minimum lengths of the lower and upper arms for males and females, respectively. Moreover, the proposed exoskeleton is supposed to be worn at about half lengths of a and b for the lower and upper arms.

The geometric input data of Table 4 have been chosen along with the input angular velocity ω_2 = 1 rad/s, and thus, running the same Matlab program, the results of Figures 9 and 10 have been obtained for the crank angles θ_2 = 300° and θ_2 = 252°, respectively.

In particular, a and b are only related to the lower (6) and upper (1) arm supports of the proposed exoskeleton mechanism, where a is about the double of d_2.

Table 4. The geometric input data in the case of Figures 9 and 10.

$r_1 = r_{31} = r_{32} = r_5 = d$ [mm]	$r_2 = r_{41} = r_{42} = r_6 = c = e$ [mm]	$r_8 = r_{11}$ [mm]	$r_9 = r_{10}$ [mm]	$d_1 = d_3$ [mm]	d_2 [mm]
70	60	18	57.90	30	117.50

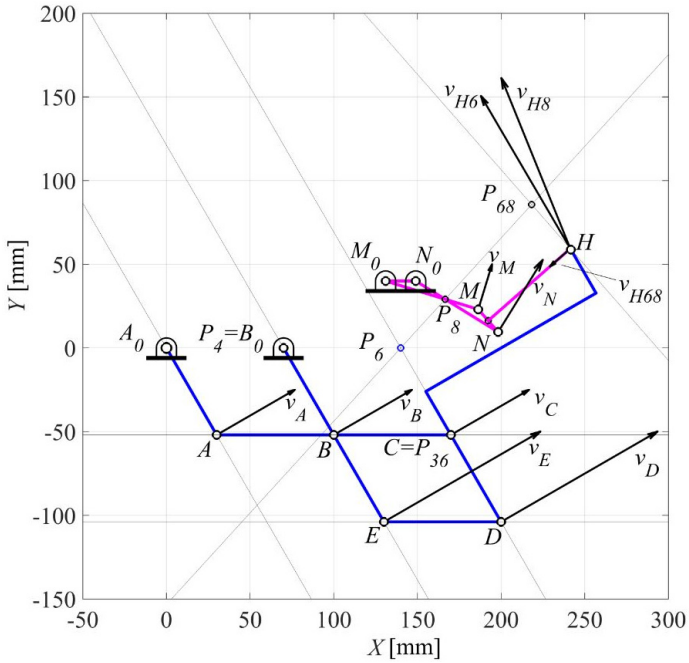

Figure 9. Ten-bar linkage for the upper-limb exoskeleton: result for a crank angle θ_2 = 300° of A_0A. (Blue and magenta colors indicate the eight-bar elbow joint exoskeleton mechanism and the crossed four-bar linkage, respectively).

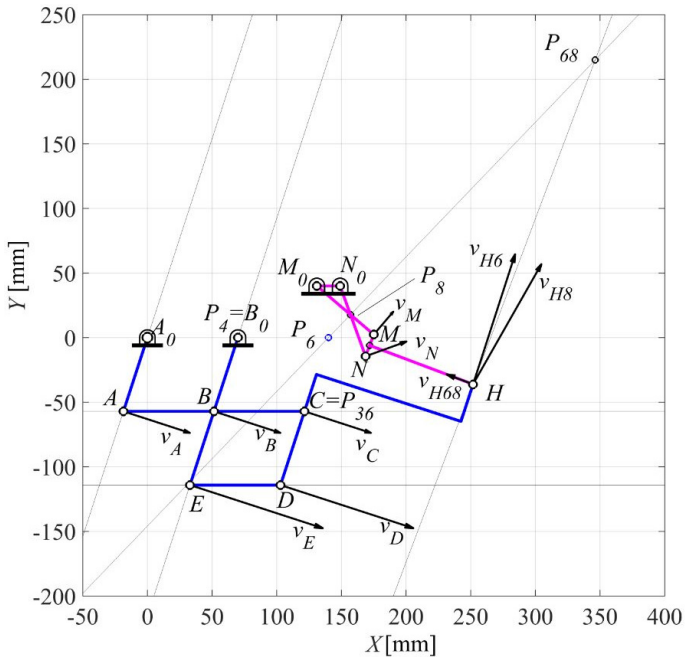

Figure 10. Result for a crank angle θ_2 = 252° of A_0A for ten-bar linkage (Blue and magenta colors indicate the eight-bar elbow joint exoskeleton mechanism and the crossed four-bar linkage, respectively).

Moreover, this design permits the wearability by different workers or persons of average sizes, thanks to the specific characteristic of auto-adaptability, which is given by the piston-glyph pair. The obtained results are reported in Tables 5 and 6. The mechanical design of the proposed ten-bar mechanism has been developed in order to build and test under a kinematic point of view the first 3D-printed planar prototype of Figure 11, which

shows a step-by-step sequence of the closing motion in comparison with the corresponding Matlab graphical results. Similarly, the whole sequence is shown in Figure 12.

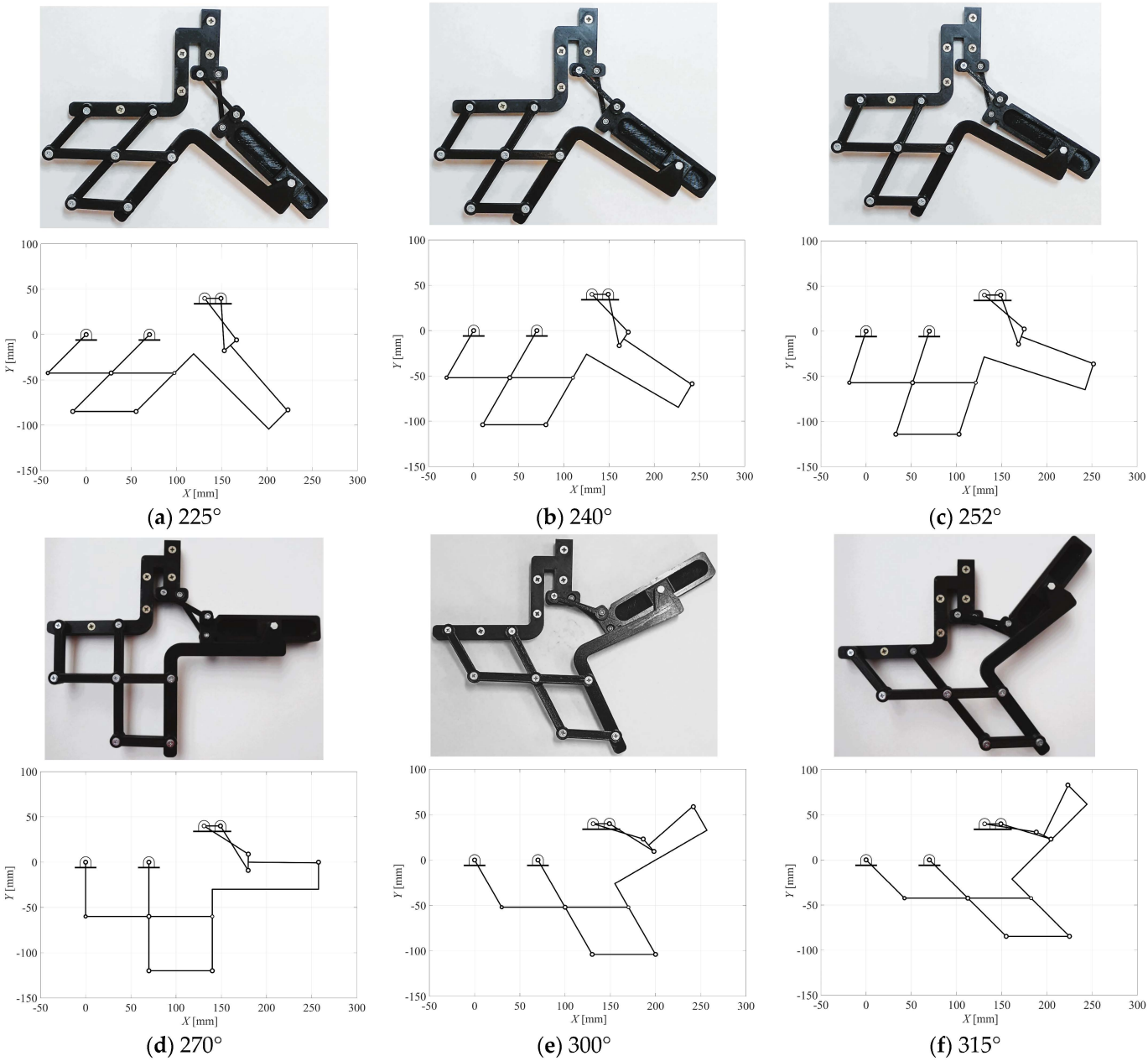

(**a**) 225° (**b**) 240° (**c**) 252°

(**d**) 270° (**e**) 300° (**f**) 315°

Figure 11. Ten-bar mechanism and 3D-printed prototype for different configurations of crank angles θ_2: (**a**) 225°; (**b**) 240°; (**c**) 252°; (**d**) 270°; (**e**) 300°; (**f**) 315°.

Table 5. Output linear velocities of all significant points for the case of Figures 9 and 10.

θ_2 [deg]	$\mathbf{v}_A = \mathbf{v}_B = \mathbf{v}_C$ [mm/s]			$\mathbf{v}_D = \mathbf{v}_E$ [mm/s]	
300	$[51.962, 30.000]^T$			$[112.583, 65.000]^T$	
252	$[57.063, -18.5410]^T$			$[13.328, -23.804]^T$	
	$\mathbf{v}_{H6}$ [mm/s]	$\mathbf{v}_{H8}$ [mm/s]	$\mathbf{v}_{H68}$ [mm/s]	$\mathbf{v}_M$ [mm/s]	$\mathbf{v}_N$ [mm/s]
300	$[-58.750, 101.758]^T$	$[-45.816, 103.288]^T$	$[-13.556, -11.892]^T$	$[9.158, 29.955]^T$	$[29.650, 47.93]^T$
252	$[36.309, 111.749]^T$	$[58.722, 103.305]^T$	$[-22.609, 8.507]^T$	$[16.74, 19.605]^T$	$[35.108, 12.69]^T$

Table 6. Output angular velocities of all moving links for the case of Figures 9 and 10.

θ_2 [deg]	$\omega_3 = \omega_5$ [rad/s]	$\omega_4 = \omega_6$ [rad/s]	ω_8 [rad/s]	ω_9 [rad/s]	ω_{10} [rad/s]	ω_{11} [rad/s]
300	0	1	1.514	0.973	0.541	−0.514
252	−0.4944	0.2183	1.0901	0.6448	0.4453	−0.0901

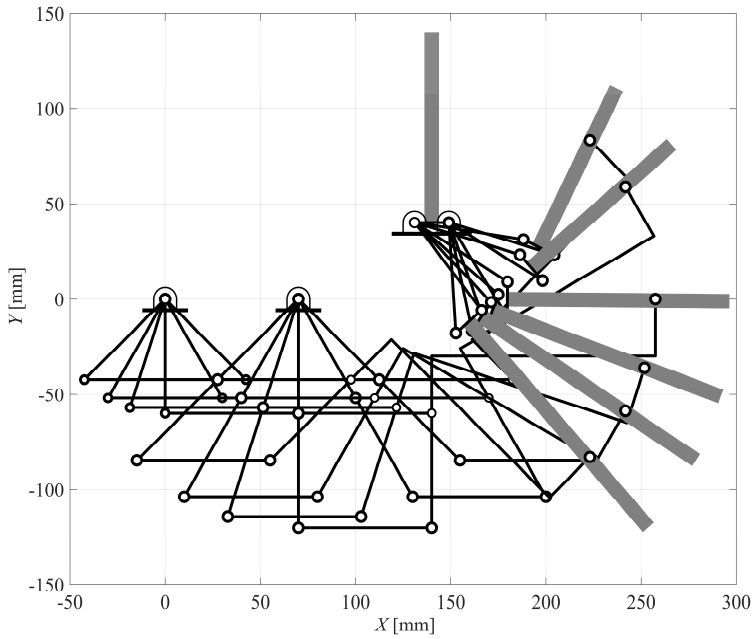

Figure 12. Whole sequence of the ten-bar mechanism closing motion.

6. Conclusions

A novel eight-bar elbow joint exoskeleton mechanism, which consists of a motorized Watt I six-bar linkage and a suitable RP dyad, has been proposed, and a suitable algorithm for the kinematic analysis of the whole one DOF ten-bar mechanism that includes the human elbow joint mechanism has been formulated for designing elbow joint exoskeleton mechanisms of different shapes and sizes. A first planar prototype has been designed and built by means of a 3D printer by considering the mean lengths of a = 241 mm and b = 338 mm of the lower and upper arms, respectively, and for males and females, and supposing to wear the proposed exoskeleton at about half lengths of them. Moreover, this design permits the wearability by different workers or persons of average sizes, thanks to the specific characteristic of auto-adaptability, while the corresponding algorithm allows to change the link sizes for analyzing the kinematic performance in different conditions and configurations. The dynamic analysis in load conditions of the proposed exoskeleton closing motion, along with the actuation and control, will be part of the next developments.

Author Contributions: Conceptualization, G.F., C.L., L.T. and J.O.; methodology, G.F., C.L. and L.T.; software, C.L.; validation, G.F., C.L. and L.T.; formal analysis, G.F. and C.L.; investigation, G.F., C.L. and L.T.; resources, G.F. and L.T.; data curation, G.F., C.L. and L.T.; writing—original draft preparation, G.F., C.L., L.T. and J.O.; writing—review and editing, G.F., C.L., L.T. and J.O.; visualization, C.L. and L.T.; supervision, G.F.; project administration, G.F.; funding acquisition, G.F. All authors have read and agreed to the published version of the manuscript.

Funding: This research activity of title EXOSKELETON (Development of an elbow/knee joint kinematic) was funded by the IIT (Italian Institute of Technology) of Genoa, within a Research Contract, which was stipulated with DICEM (Dept. of Civil and Mechanical Engineering) of the University of Cassino and Southern Lazio (Italy) in the years 2018/19.

Data Availability Statement: The original contributions presented in the study are included in the article, further inquiries can be directed to the corresponding author.

Conflicts of Interest: The authors declare no conflicts of interest.

References

1. Zatsiorsky, V.M. *Kinematics of Human Motion*; Human Kinetics: Champaign, IL, USA, 1998.
2. Klopčar, N.; Tomšič, M.; Lenarčič, J. A kinematic model of the shoulder complex to evaluate the arm-reachable workspace. *J. Biomech.* **2007**, *40*, 86–91. [CrossRef] [PubMed]
3. Rosen, J.; Perry, J. Upper limb powered exoskeleton. *Int. J. Humanoid Robot.* **2007**, *4*, 529–548. [CrossRef]
4. Naidu, D.; Stopforth, R.; Bright, G.; Davrajh, S. A 7 DOF exoskeleton arm: Shoulder, elbow, wrist and hand mechanism for assistance to upper limb disabled individuals. In Proceedings of the IEEE Africon '11, Victoria Falls, Zambia, 10 November 2011; pp. 1–6.
5. Kiguchi, K.; Rahman, M.H.; Sasaki, M.; Teramoto, K. Development of a 3DOF mobile exoskeleton robot for human upper-limb motion assist. *Robot. Auton. Syst.* **2008**, *56*, 678–691. [CrossRef]
6. Wang, X.; Song, Q.; Wang, X.; Liu, P. Kinematics and dynamics analysis of a 3-DOF upper-limb exoskeleton with an internally rotated elbow joint. *Appl. Sci.* **2018**, *8*, 464. [CrossRef]
7. Lu, J.; Chen, W.; Tomizuka, M. Kinematic design and analysis of a 6-DOF upper limb exoskeleton model for a brain-machine interface study. *IFAC Proc. Vol.* **2013**, *46*, 293–300. [CrossRef]
8. Chen, Y.; Ge, L.; Yanhe, Z.; Jie, Z.; Hegao, C. Design of a 6-DOF upper limb rehabilitation exoskeleton with parallel actuated joints. *Bio-Med. Mater. Eng.* **2014**, *24*, 2527–2535. [CrossRef] [PubMed]
9. Caldwell, D.; Tsagarakis, N.; Kousidou, S.; Costa, N.; Sarakoglou, I. "Soft" exoskeletons for upper and lower body rehabilitation—Design, control and testing. *Int. J. Humanoid Robot.* **2014**, *4*, 549–573. [CrossRef]
10. Vertechy, R.; Frisoli, A.; Dettori, A.; Solazzi, M.; Bergamasco, M. Development of a new exoskeleton for upper limb rehabilitation. In Proceedings of the 2009 IEEE International Conference on Rehabilitation Robotics, Kyoto, Japan, 23–26 June 2009; pp. 188–193.
11. Tsai, B.C.; Wang, W.W.; Hsu, L.C.; Fu, L.C.; Lai, J.S. An articulated rehabilitation robot for upper limb physiotherapy and training. In Proceedings of the 2010 IEEE/RSJ International Conference on Intelligent Robots and Systems, Taipei, Taiwan, 18–22 October 2010; pp. 1470–1475.
12. Lugo-Villeda, M.A.; Ruiz-Sanchez, F.J.; Dominguez-Ramirez, O.A.; Parra-Vega, V. Robotic Design of an Upper Limb Exoskeleton for Motion Analysis and Rehabilitation of Paediatric Neuromuscular Disorders. In *Converging Clinical and Engineering Research on Neurorehabilitation. Biosystems & Biorobotics*; Springer: Berlin/Heidelberg, Germany, 2013; Volume 1, pp. 265–269.
13. Maciejasz, P.; Eschweiler, J.; Gerlach-Hahn, K.; Jansen-Troy, A.; Leonhardt, S. A survey on robotic devices for upper limb rehabilitation. *J. NeuroEngineering Rehabil.* **2014**, *11*, 3. [CrossRef] [PubMed]
14. Zeiaee, A.; Soltani-Zarrin, R.; Langari, R.; Tafreshi, R. Design and kinematic analysis of a novel upper limb exoskeleton for rehabilitation of stroke patients. In Proceedings of the 2017 International Conference on Rehabilitation Robotics (ICORR), London, UK, 17–20 July 2017; pp. 759–764.
15. Gull, M.A.; Bai, S.; Bak, T. A Review on Design of Upper Limb Exoskeletons. *Robotics* **2020**, *9*, 16. [CrossRef]
16. Tsagarakis, N.; Caldwell, D.G.; Medrano-Cerda, G.A. A 7 DOF pneumatic muscle actuator (PMA) powered exoskeleton. In Proceedings of the 8th IEEE International Workshop on Robot and Human Interaction. RO-MAN '99 (Cat. No.99TH8483), Pisa, Italy, 27–29 September 1999; pp. 327–333.
17. Stanišić, M.M.; Goehler, C.M. Reproducing human arm motion using a kinematically coupled humanoid shoulder-elbow complex. *Appl. Bionics Biomech.* **2008**, *5*, 175–185. [CrossRef]
18. Xiao, Y.; Zhu, Y.; Wang, X.; Zhao, Y.; Ding, Q. Configuration optimization and kinematic analysis of a wearable exoskeleton arm. In Proceedings of the 2017 International Conference on Robotics and Automation Sciences (ICRAS), Hong Kong, China, 26–29 August 2017; pp. 124–128.
19. Ma, R.; Tang, Z.; Gao, X.; Ni, W. Mechanism Design and Kinematics Analysis of an Original Cable-driving Exoskeleton Robot. In Proceedings of the 2018 2nd IEEE Advanced Information Management, Communicates, Electronic and Automation Control Conference (IMCEC), Xi'an, China, 25–27 May 2018; pp. 1869–1874.
20. Dežman, M.; Asfour, T.; Ude, A.; Gams, A. Mechanical design and friction modelling of a cable-driven upper-limb exoskeleton. *Mech. Mach. Theory* **2022**, *171*, 104746. [CrossRef]
21. Bai, S.; Christensen, S.; Islam, M.R.U. An upper-body exoskeleton with a novel shoulder mechanism for assistive applications. In Proceedings of the 2017 IEEE International Conference on Advanced Intelligent Mechatronics (AIM), Munich, Germany, 3–7 July 2017; pp. 1041–1046.
22. Figliolini, G.; Lanni, C.; Kaur, R. Kinematic synthesis of spherical four-bar linkages for five-poses rigid body guidance. In *Advances in Mechanism and Machine Science*; Uhl, T., Ed.; IFToMM WC 2019. Mechanisms and Machine Science; Springer: Cham, Switzerland, 2019; Volume 73, pp. 639–648. [CrossRef]
23. Bardi, E.; Gandolla, M.; Braghin, F.; Resta, F.; Pedrocchi, A.L.G.; Ambrosini, E. Upper limb soft robotic wearable devices: A systematic review. *J. NeuroEngineering Rehabil.* **2022**, *19*, 87. [CrossRef] [PubMed]
24. Matsumoto, Y.; Amemiya, M.; Kaneishi, D.; Nakashima, Y.; Seki, M.; Ando, T.; Kobayashi, Y.; Iijima, H.; Nagaoka, M.; Fujie, M.G.; et al. Development of an elbow-forearm interlock joint mechanism toward an exoskeleton for patients with essential tremor. In Proceedings of the 2014 IEEE/RSJ International Conference on Intelligent Robots and Systems, Chicago, IL, USA, 14–18 September 2014; pp. 2055–2062.

25. Manna, S.K.; Dubey, V.N. A mechanism for elbow exoskeleton for customised training. In Proceedings of the 2017 International Conference on Rehabilitation Robotics (ICORR), London, UK, 17–20 July 2017; pp. 1597–1602.
26. Canesi, M.; Xiloyannis, M.; Ajoudani, A.; Biechi, A.; Masia, L. Modular one-to-many clutchable actuator for a soft elbow exosuit. In Proceedings of the 2017 International Conference on Rehabilitation Robotics (ICORR), London, UK, 17–20 July 2017; pp. 1679–1685.
27. Song, H.; Kim, Y.S.; Yoon, J.; Yun, S.H.; Seo, J.; Kim, Y.J. Development of Low-Inertia High-Stiffness Manipulator LIMS2 for High-Speed Manipulation of Foldable Objects. In Proceedings of the 2018 IEEE/RSJ International Conference on Intelligent Robots and Systems (IROS), Madrid, Spain, 1–5 October 2018; pp. 4145–4151.
28. Zhang, S.; Fu, Q.; Guo, S.; Fu, Y. A Telepresence System for Therapist-in-the-Loop Training for Elbow Joint Rehabilitation. *Appl. Sci.* **2019**, *9*, 1710. [CrossRef]
29. Liu, Y.; Wang, D.; Yang, S.; Liu, J.; Hao, G. Design and experimental study of a passive power-source-free stiffness-self-adjustable mechanism. *Front. Mech. Eng.* **2021**, *16*, 32–45. [CrossRef]
30. Beadle, C.W.; O'Brien, M.E. Kinematic analysis of the human elbow. *Orthot. Prosthet.* **1976**, *30*, 31–32.
31. Freudenstein, F.; Woo, L.S. Kinematics of the human knee joint. *Bull. Math. Biophys.* **1969**, *31*, 215–232. [CrossRef] [PubMed]
32. Tomassi, L.; Lanni, C.; Figliolini, G. A Novel Design Method of Four-Bar Linkages Mimicking the Human Knee Joint in the Sagittal Plane. In *The International Conference of IFToMM ITALY*; Niola, V., Gasparetto, A., Quaglia, G., Carbone, G., Eds.; Springer International Publishing: Cham, Switzerland, 2022; pp. 586–592. [CrossRef]
33. Figliolini, G.; Lanni, C.; Sorli, M. Kinematic analysis and centrodes between rotating tool with reciprocating motion and workpiece. In *The International Conference of IFToMM ITALY*; Niola, V., Gasparetto, A., Quaglia, G., Carbone, G., Eds.; Springer International Publishing: Cham, Switzerland, 2022; pp. 54–60. [CrossRef]
34. Lanni, C.; Figliolini, G.; Tomassi, L. Higher-Order Centrodes and Bresse's Circles of Slider-Crank Mechanisms. In Proceedings of the ASME 2023 IDETC-CIE2023, Boston, MA, USA, 20–23 August 2023; Volume 8, article number v008t08a012. [CrossRef]
35. Figliolini, G.; Lanni, C.; Cirelli, M.; Pennestrì, E. Kinematic Properties of nth-order Bresse Circles Intersections for a Crank-Driven Rigid Body. *Mech. Mach. Theory* **2023**, *190*, 105445. [CrossRef]
36. Gordon, C.G.; Churchill, T.; Clauser, C.E.; Bradtmiller, C.B.; McConville, J.T.; Tebbetts, I.; Walker, R.A. *1988 Anthropometric Survey of U.S. Personnel: Summary Statistics*; Technical Report Natick/TR-89/044; Anthropology Research Project, Inc.: Yellow Springs, OH, USA, 1989.

Disclaimer/Publisher's Note: The statements, opinions and data contained in all publications are solely those of the individual author(s) and contributor(s) and not of MDPI and/or the editor(s). MDPI and/or the editor(s) disclaim responsibility for any injury to people or property resulting from any ideas, methods, instructions or products referred to in the content.